RASMUSSEN, S.B., HAMMA, H., ERIKSEN, K.M., HATEM, G., GAUNE-ESCARD, M. and FEHRMANN, R. Physico-chemical properties and transition metal complex formation in alkali pyrosulfate and hydrogen sulfate melts. *VII International Conference on Molten Slags Fluxes and Salts,* The South African Institute of Mining and Metallurgy, 2004.

Physico-chemical properties and transition metal complex formation in alkali pyrosulfate and hydrogen sulfate melts

S.B. RASMUSSEN*, H. HAMMA†, K.M. ERIKSEN*, G. HATEM†, M. GAUNE-ESCARD‡ and R. FEHRMANN*.

*Department of Chemistry and ICAT (Interdisciplinary Research Center for Catalysis), Technical University of Denmark,
†Laboraoire TECSEN UMR-CNRS, Marseille, France
‡Institut Universitaire des Systemes Thermiques Industriels Technopole, Marseille, France

The molten salts $M_2S_2O_7$ and $MHSO_4$, the binary molten salt systems $M_2S_2O_7$-$MHSO_4$ and the molten salt-gas systems $M_2S_2O_7$-V_2O_5 and $M_2S_2O_7$-M_2SO_4-V_2O_5 (M = Na, K, Rb, Cs) in O_2, SO_2 and Ar atmospheres have been investigated by thermal methods like calorimetry, Differential Enthalpic Analysis (DEA) and Differential Scanning Calorimetry (DSC). Fundamental thermodynamic data like temperatures and molar heats of solid-solid transition and fusion, phase diagrams, heat capacities of solids and liquids, heat of mixing, and heats of complex formation have been obtained and are reviewed here. Also EPR spectroscopic evidence of V(IV) complexes and their structure are reported and the results are discussed in relation to the mechanism of SO_2 oxidation by V_2O_5 based industrial catalysts.

Keywords: Alkali pyrosulfates, alkali hydrogen sulfates, vanadium pentoxide, EPR spectroscopy, complex formation

Introduction

The molten salt-gas system $M_2S_2O_7$-$MHSO_4$-M_2SO_4-V_2O_5 / SO_2-O_2-SO_3-H_2O-N_2 (M = alkali) at 400–600ºC is considered a realistic model of the SO_2 oxidation catalyst under various conditions of industrial operation[1]. Traditional industrial SO_2 oxidation catalysts have molar ratios in the range M/V = 2–4, where M is usually a mixture of K and Na. In some cases also Cs is added in order to improve the activity at lower temperatures, i.e. below 420ºC, where precipitation of low soluble V(IV) and V(III) compounds has been shown to cause catalyst deactivation[1-3]. The molten salt mixture $M_2S_2O_7$-$MHSO_4$ is also an excellent solvent for the dissolution of transition metal oxides.

In the light of this we are currently investigating fundamental physico-chemical, redox and complex chemical properties as well as the catalytic activity of the general catalyst model system or part systems. We utilize spectroscopic, electrochemical and magnetic methods as well as thermal methods Results of the latter method are reviewed here, focusing on the alkali metals Na, K, Rb and Cs, since Li is known not to form a stable pyrosulfate.

Experimental

Chemicals

Pure $M_2S_2O_7$ salts are either not commercially available (Rb, Cs) or seriously contaminated by hydrogen sulfates (Na, K) due to their hygroscopicity. Therefore, pure and dry $M_2S_2O_7$ was synthesized by thermal decomposition in dry N_2 atmosphere of commercial $M_2S_2O_8$ (Merck, p.a.), in the case of Na and K, while the non-commercially available peroxo-disulfates $Rb_2S_2O_8$ and $Cs_2S_2O_8$ were synthesized in the laboratory as earlier described[1,4]. The commercial available $NaHSO_4$ and $KHSO_4$ (Merck, suprapur (99%)) were dried at 110ºC while the non-commercial available $RbHSO_4$ and $CsHSO_4$ were synthesized by adding carefully weighed amounts of water to the respective pyrosulfates in ampules. The ampules were then sealed and equilibrated by slow step-wise heating to 230–250 ºC. The purity was checked by Raman spectroscopy[5] on the molten salt showing less than 0.5% residual pyrosulfate. All handlings of the hygroscopic alkali pyrosulfates and hydrogen sulfates were performed in a glovebox with a water content of less than around 5 ppm. All chemicals were kept on ampules, only opened in the glovebox, and resealed immediately after use.

The non-hygroscopic V_2O_5 (Cerac, pure (99.9%)) and alkali sulfates M_2SO_4 (Merck, p.a.) could be kept outside the glovebox and used without further treatment. Commercial gases of O_2, N_2, Ar, SO_2 and air were used and, when necessary, dried through P_2O_5 containing glass columns.

Thermal measurements

The temperatures of the phase transitions, solid-solid or solid-liquid, and the heat involved in these transitions have been measured by DEA (Differential Enthalpic Analysis) with a Calvet micro calorimeter. This apparatus has been described previously[6,7]. The heat, Q, involved during the

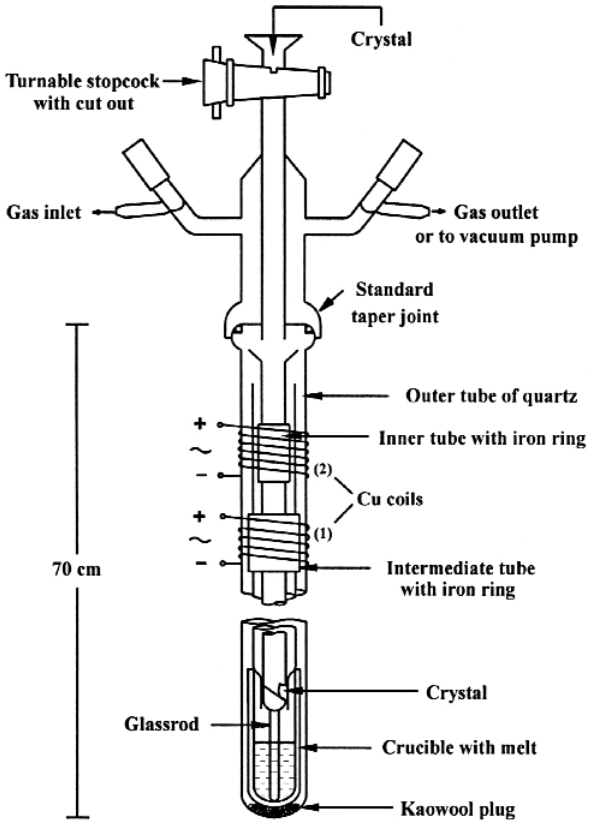

Figure 1.Calorimetric device allowing indirect addition in a controlled atmosphere and agitation of the melt. Onset of current to coil (1) elevates the intermediate tube and the thermal equilibrated crystal drops into the melt at the same temperature. By varying the current to coil (2) the inner tube moves up and down whereby the glass rod agitates the melt[26]

phase transition is linked to the area, *S*, of the thermogram by the linear relation: $Q = KS$, where K is the calorimeter constant. This constant is determined in a separate experiment with the same heating rate on a sample of lead. Temperature and enthalpy of melting of lead are[8] T_{fus} = 600 K and $\Delta_{fus}H$ = 4.81 kJ mol^{-1}. The heat of mixing of the investigated systems was measured in the Calvet micrometer. Two methods were used: the direct drop and the indirect drop method. The device used for the indirect method is shown in Figure 1. By this method the added crystals of V_2O_5 were thermally equilibrated just above and at the same temperature as the melt.

Then, by applying current to coil (1), the crystal dropped into the melt and the exchanged heat recorded and integrated graphically or by a connected data acquisition computer. Alternatively, the experiments were carried out by the direct drop method essentially performed by a set-up as shown in Figure 1, but omitting the intermediate tube. The calorimeter was calibrated at the end of each experimental series by direct drop of pre-weighted gold bullets to the melt. The partial enthalpy of liquid-liquid mixing $\Delta H_{part}(A)$, when a solid (A) is dropped from room temperature, T_{amb}, into a liquid at temperature T and at constant pressure, is given by Equation [1]:

$$\Delta H_{part}(A) = \qquad [1]$$

where Δh_{exp} is the experimentally measured heat, n^A is the number of moles of component A added by each experiment, $C_p(A)$ is the heat capacity of A and $\Delta H_f(A, T)$ is the molar enthalpy of fusion of A extrapolated to the experimental temperature T. The molar heat of fusion of V_2O_5 (m.p. 670ºC), was found to be 61.65 kJ/mol and 62.16 kJ/mol, respectively at 430ºC and 470ºC, by extrapolation of the data in reference 9. Heat capacity measurements were carried out with a Setaram DSC 121 differential scanning calorimeter. The apparatus and the measuring procedure have been previously described in detail[10]. The measuring method used was the so-called 'step-method', developed by Setaram[11]. Quartz cells of 7 mm in diameter and 15 mm in length were filled in the glovebox, sealed under vacuum and then placed in the calorimeter. Measurements were performed by heating steps of 5 K followed by 400 s isothermal delay. The heating rate was 2 K min^{-1}. All experiments were started at 300 K and performed up to 750–800 K.

EPR Spectroscopy

Mixtures of $M_2S_2O_7$ and M_2SO_4 were prepared by melting and mixing the components in a sealed ampoule. V_2O_5 was added to this mixture at a M/V ($M_2S_2O_7/V_2O_5$) molar ratio of 40. The chemicals were filled into a quartz ampule (diameter = 12 mm, 300 mm length) in the glovebox and sealed immediately under *ca.* 0.7 bar SO_2. The sealed ampules were equilibrated for at least 100 hours just above the melting point of the mixture, i.e. 400–460ºC dependent on the type of alkali metal. From the furnace the ampules were dropped directly into icy water. After quenching, the ampules were cut open in the glovebox and some of the mixture ground and transferred to quartz capillary tubes (2.0 mm outer diameter, 0.5 mm wall thickness). The samples were sealed under vacuum. Samples with other M/V ratios were made by dilution of the M/V = 40 mixture with a premixed $M_2S_2O_7$-M_2SO_4 mixture.

Table I. Thermal properties of $M_2S_2O_7$ (M = Na, K, Rb, Cs). Temperatures, enthalpies and entropies of fusion, coefficients for the linear equations $C_p(s) = A + BT$ for the heat capacities of the solid state, heat capacities of the liquid state, associate temperature ranges and molar volumes

	T_{fus} (K)	$\Delta_{fus}H$ (J mol^{-1})	$\Delta_{fus}S^b$ (J mol^{-1} K^{-1})	$C_p(s)$ (J mol^{-1} K^{-1}) A	B	T range (K)	$C_p(l)$ (J mol^{-1} K^{-1})	T range (K)	$V_m(T_{fus})$ (cm^3 mol^{-1})
$Na_2S_2O_7$	675	41700	62	110.2(36)	0.187(8)	300–590	244.8(10)	680–720	102.14
$K_2S_2O_7$ [a]	692	21200	31	134.7(10)	0.177(7)	300–590	267(2)	680–717	121.10
$Rb_2S_2O_7$	723	17800	25	207.4(12)	0.057(4)	300–700	272.2(18)	724–757	122.72
$Cs_2S_2O_7$	734	19500	27	147.5(19)	0.21(10)	300–710	292.3(43)	717–777	149.15

[a] $\Delta trans H\alpha \rightarrow \beta$(591 K) = 21800 J mol^{-1}; Cp(s) = 260.4 J mol^{-1} K^{-1}; T = 591–692 K.
[b] Calculated as $\Delta H_{fus}/T_{fus}$.

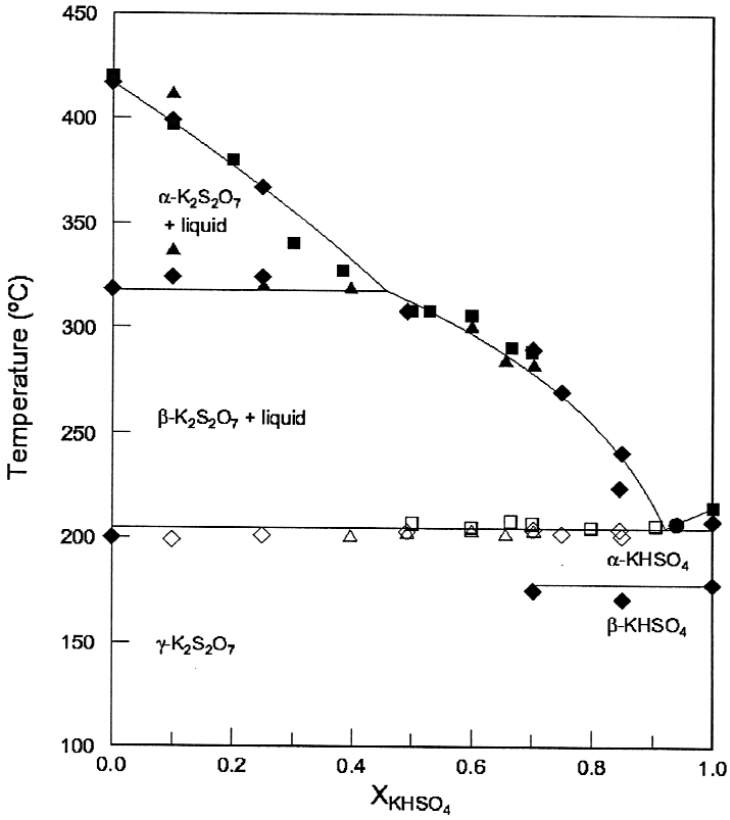

Figure 2. Phase diagram of the $K_2S_2O_7$-$KHSO_4$ system obtained from conductivity (■), DEA (◆), TA (Δ), and NIR (●) measurements. Open symbols indicate the melting point of the eutectic. The liquidus line and the composition and melting temperature of the eutectic mixture are calculated by assuming ideality of the binary system[13]

Samples without SO_4^{2-}-saturation are sensitive to the decomposition of the solvent melt, due to the high vapour pressure of SO_3, which causes SO_4^{2-}-contamination of the $M_2S_2O_7$ -especially at higher temperatures. The mixing procedure was the same as in the previous case, except that the samples were not remelted and requenched after being transferred to the capillaries as in the case of the $M_2S_2O_7$-M_2SO_4-(sat)V_2O_5/SO_2(g) system. No spectra of molten samples were recorded. It was not possible to record well resolved spectra with M/V ratios smaller than 160, the spectra smeared out due to increased spin-spin relaxation. The EPR spectra were recorded on a Bruker EMX spectrometer with a 12 kW 10″; magnet. Room temperature Xband spectra were recorded with a Bruker ER4102ST cavity. High temperature X-band spectra were recorded with a Bruker ER4114HT cavity whereas the room temperature Q-band spectra were obtained with a Bruker ER5106Q cavity.

Results and discussion

$M_2S_2O_7$ (M = Na, K, Rb, Cs)

The data obtained on the alkali pyrosulfates are given in Table I. The coefficient for the heat capacity of solid $K_2S_2O_7$ was erroneously given in degrees Celsius in our previous publication[12] on this subject.

From the thermograms (DEA) obtained[13] on $K_2S_2O_7$ and $KHSO_4$ the solid-solid $\beta \rightarrow \alpha$ transition is found for $K_2S_2O_7$ at 591 K and the temperature of fusion at 690 K, which, however, based on several measurements of the electrical conductivity (at the phase transition) is considered actually to be 692 K as given in Table I. Most of the information on the alkali pyrosulfates could not be found in the literature before or deviate largely from the values given here, e.g. the melting temperature of $Cs_2S_2O_7$ is 734 K compared to 553 K, the only value published previously[14].

The discrepancies are most probably due to serious contamination by hydrogensulfates due to the hygroscopic properties of the alkali pyrosulfates. For $K_2S_2O_7$ the entropy of the $\beta \rightarrow \alpha$ solid-solid transition at 591 K is found to be 37 $Jmol^{-1}$ K^{-1}, i.e. of the same size as the entropy of fusion of 31 $Jmol^{-1}$-K^{-1} found for at $K_2S_2O_7$. The sum of 68 $Jmol^{-1}$ K^{-1} is comparable to the entropy of fusion for $Na_2S_2O_7$ where no low temperature solid-solid transition is found. Therefore, the structure of β-$K_2S_2O_7$ and $Na_2S_2O_7$ are probably very similar while the structures of $Rb_2S_2O_7$ and $Cs_2S_2O_7$ probably are similar to the structure of α-$K_2S_2O_7$ judged from their comparable melting entropies. However, only the X-ray structure of $K_2S_2O_7$ is reported in the literature, but very recently we have revealed[15] from room temperature powder XRD on $Na_2S_2O_7$ that the two salts indeed have a very similar structure.

In addition to the thermal investigations, results from parallel density measurements[12] are given in Table I in the form of the molar volume of the liquids at the melting temperature. A steady increase of the molar volume by increasing size of the cation is expected and indeed observed.

$MHSO_4$ (M = Na, K, Rb, Cs)

As for the alkali pyrosulfates DEA has been performed on the acid sulfates[13]. As for $K_2S_2O_7$ the temperature of fusion of $KHSO_4$ has been determined more accurately by conductometric measurements to be 488 K. This value and

Table II. Thermal properties of $MHSO_4$ (M = Na, K, Rb, Cs). Temperatures, enthalpies and entropies of fusion, coefficients for the linear equations $C_p(s) = A + BT$ for the heat capacities of the solid state, heat capacities of the liquid state and associate temperature ranges

	T_{fus} (K)	$\Delta_{fus}H$ ($J\ mol^{-1}$)	$\Delta_{fus}S$ ($J\ mol^{-1}\ K^{-1}$)	$C_p(s)$ ($J\ mol^{-1}\ K^{-1}$) A	B	T range (K)	T range ($J\ mol^{-1}\ K^{-1}$)	$C_p(l)$ (K)	T range
$NaHSO_4$	455	17300	38	124.7	0	298–455	246	455–500	
$KHSO_4$ [a]	488	16600	34	-62.5	0.56	298–488	287	488–545	
$RbHSO_4$ [b]	479	12770	27						
$CsHSO_4$ [c]	491	9580	20						

[a] $\Delta_{trans}H(451\ K) = 2110\ J\ mol^{-1}$
[b] $\Delta_{trans}H(472\ K) = 3855\ J\ mol^{-1}$
[c] $\Delta_{trans}H(451\ K) = 6790\ J\ mol^{-1}$

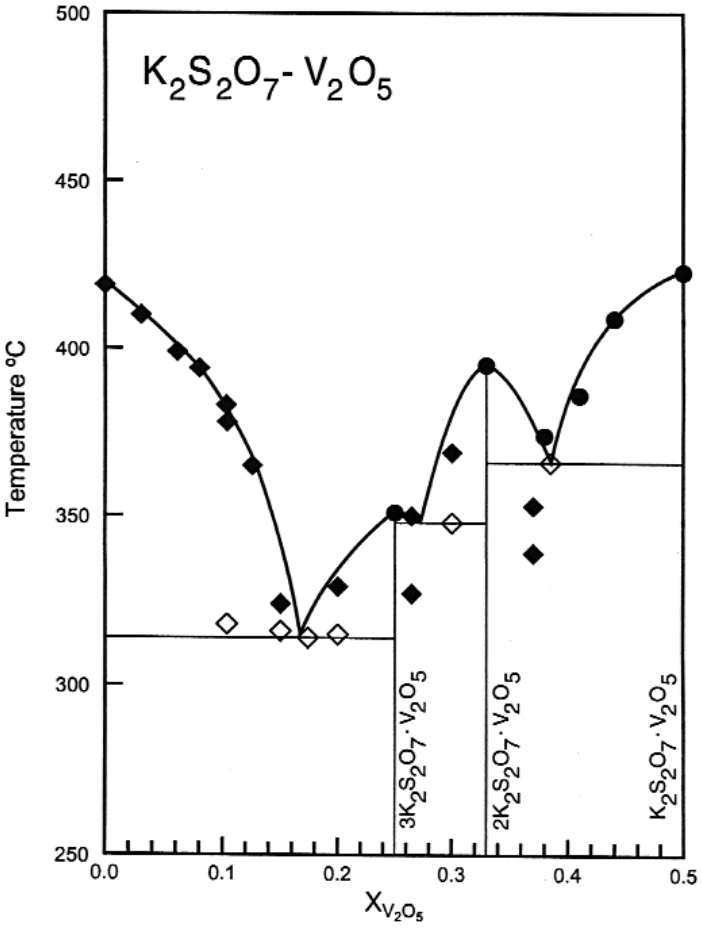

Figure 3. Phase diagram of $K_2S_2O_7$-V_2O_5 system obtained from conductivity (◆) and K NMR spectroscopic measurements (●). Open symbols indicate the melting temperature of a eutectic phase. The compositions of the possible compounds formed in the system are as indicated[18].

other measured thermal parameters for the alkali hydrogen sulfates are shown in Table II. Again, only very little information, e.g. temperatures of fusion of $NaHSO_4$ and $KHSO_4$ have earlier been given in the literature or a large deviation is found compared to our values.

$M_2S_2O_7$-$MHSO_4$ (M = Na, K, Rb, Cs)

The phase diagrams of these binary systems are currently being investigated by us, using thermal, electrochemical and spectroscopic methods. The results for the $K_2S_2O_7$-$KHSO_4$ system[13] is shown in Figure 3 as an example. The phase diagram shows considerable variations above = 0.45 from the diagram of Hagisawa and Takai[16], which was obtained from differential enthalpic analysis only.

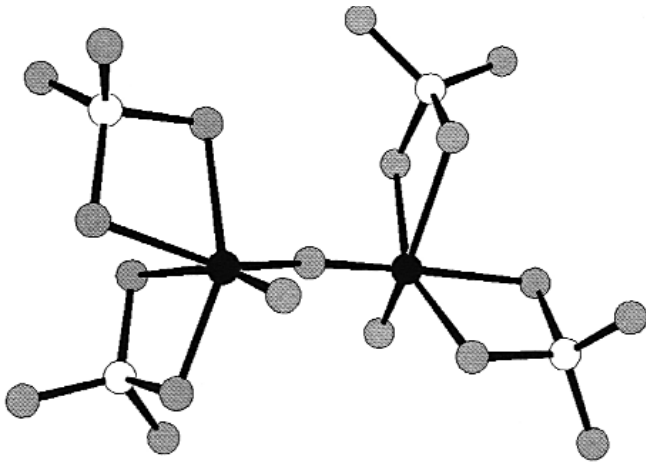

Figure 4. Structure of $(VO)_2O(SO_4)_4^{4-}$, V (dark circles), S (open circles), O (gray circles)

The diagram of Cambi and Bozza[17] also deviates dramatically from ours, i.e., up to 55 K lower liquidus temperatures were found by these authors, probably because their DTA measurements were performed by cooling, leading to large subcooling before crystallization. Thermodynamic calculations show that the heat of the $\alpha \rightarrow \beta$ transition at 591 K for $K_2S_2O_7$ is so large that the liquidus curve in the vicinity of the temperature, corresponding to = 0.45 in the phase diagram, will exhibit a marked change in the slope. The eutectic composition could not be found accurately by the conductivity or thermal methods, but was alternatively found by spectrophotometry since O-H vibrations absorb rather strongly in the near infrared region. From spectra of the eutectic melt and a series of standards, prepared around the eutectic, the composition was found with high precision[13]. All of the diagrams exhibit simple eutectic systems with a composition of the eutectics rather close to the pure alkali hydrogensulfate, i.e. = 0.98, 0.94, 0.87 and 0.84 for M = Na, K, Rb and Cs respectively[13]. The measurements and calculations point for both systems to an ordered liquid, most probably due to oscillating H-bonding between the species HSO_4^- and $S_2O_7^{2-}$, dominating the liquid as illustrated by the equation:

Table III. Possible reactions and reaction enthalpies of the molten systems $M_2S_2O_7$-V_2O_5 and $M_2S_2O_7$-M_2SO_4(sat)-V_2O_5 (M = K and Cs) in Ar or SO_2 gas atmospheres[a]

Liquid-liquid reactions	K (kJ mol^{-1})	Cs (kJ mol^{-1})
	Experimental enthalpies	
$V_2O_5 + 2S_2O_7^{2-} \rightarrow (VO)_2O(SO_4)_4^{4-}$	-89.2±1	-89.1±1
$V_2O_5 + S_2O_7^{2-} + 2SO_4^{2-} \rightarrow 2VO_2(SO_4)_2^{3-}$	-124±12	-166±12
$V_2O_5 + 2S_2O_7^{2-} + SO_2 \rightarrow 2VO(SO_4)_2^{2-} + SO_3$	-180±20	-176±7
$V_2O_5 + S_2O_7^{2-} + 3SO_4^{2-} + SO_2 \rightarrow 2VO(SO_4)_3^{4-}$	-208±20	-228±7
	Calculated enthalpies	
$(VO)_2O(SO_4)_4^{4-} + 2SO_4^{2-} \rightarrow 2VO_2(SO_4)_2^{3-} + S_2O_7^{2-}$	-35±12	-77±12
$(VO)_2O(SO_4)_4^{4-} + SO_2 \rightarrow 2VO(SO_4)_2^{2-} + SO_3$	-91±20	-87±7
$2VO_2(SO_4)_2^{3-} + SO_4^{2-} + SO_2 \rightarrow 2VO(SO_4)_3^{4-}$	-84±23	-62±10
$2VO(SO_4)_2^{2-} + 3SO_4^{2-} + SO_3 \rightarrow 2VO(SO_4)_3^{4-} + S_2O_7^{2-}$	-28±28	-52±10
[a] Reaction temperatures: K: 703 K, Cs: 743 K.		

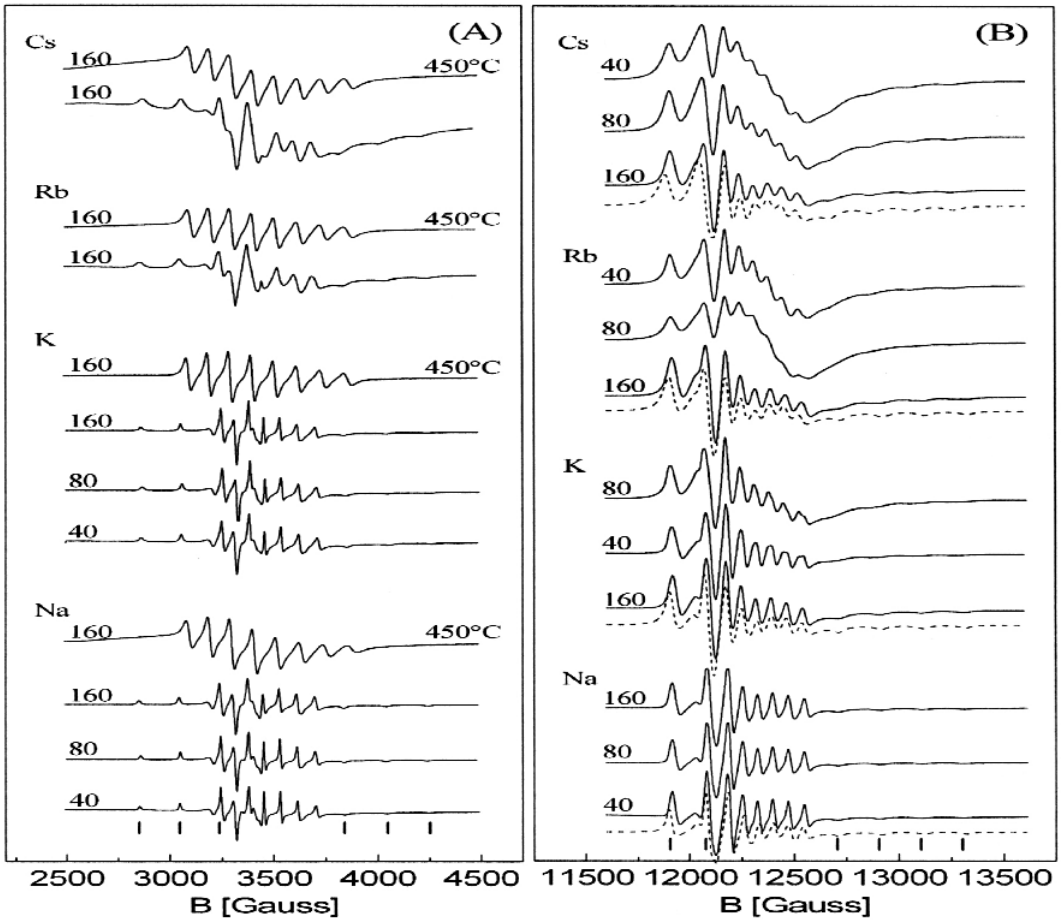

Figure 5. X-band (A) and Q-band (B) EPR spectra of $VO(SO_4)_3^{4-}$ in the $M_2S_2O_7$-M_2SO_4(sat)-V_2O_5/SO_2(g) system with M/V = 40, 80 and 160 (M = Na, K , Rb and Cs). All spectra are recorded at room temperature except for the indicated M/V= 160 samples recorded at 450–460°C in the X-band. Simulated spectra are shown strippled

$$SO_3 \; {}^{O-SO_3\ldots H}_{(HSO_4^-)} \; {}^{O-SO_3\ldots SO_3}_{(S_2O_7^{2-})} \; {}^{O-SO_3\ldots H}_{(HSO_4^-)} \; O-SO_3 \qquad [2]$$

All of the $M_2S_2O_7$-$MHSO_4$ systems exhibit melting temperatures of the eutectics some 250 K lower than the temperature of fusion of the alkali pyrosulfates, $M_2S_2O_7$ (M=Na, K, Rb, Cs), which may prove interesting for the design of low melting solvents for transition metal oxides.

$M_2S_2O_7$-V_2O_5 (M = Na, K, Rb, Cs)

The phase diagrams of these binary systems have been obtained by us for M = K, Rb and Cs[4,18-19] while the system based on Na is thermally unstable, decomposing to sulfates and gaseous SO_3 by increasing temperature and content of V_2O_5. Thus the pure Na-system could not be studied. The other systems have been studied by electrical conductivity measurements in various combinations with thermal and spectroscopic techniques. An example is shown in Figure 3 for M = K[18].

The phase diagram of the $K_2S_2O_7$-V_2O_5 system exhibits three maxima corresponding to the formation of compounds with the stoichiometry $3K_2S_2O_7 \bullet V_2O_5$, $2K_2S_2O_7 \bullet V_2O_5$, and $K_2S_2O_7 \bullet V_2O_5$. These compounds can most probably be attributed to, respectively, the formulas $K_3VO_2SO_4S_2O_7$, $K_4(VO)_2O(SO_4)_4$ and KVO_2SO_4 judged from previous[20] single crystal X-ray investigations on the Cs-salt $Cs_4(VO)_2O(SO_4)_4$ and ongoing X-ray investigations[21] on the analogous K and Rb salts and the compound $CsVO_2SO_4$.

The phase diagrams of the $Rb_2S_2O_7$-V_2O_5 system and the $Cs_2S_2O_7$-V_2O_5 system, both exhibit only one maximum at = 0.33 corresponding to the formation of the compound $M_4(VO)_2O(SO_4)_4$ while the compound MVO_2SO_4 most probably might be formed in both systems at = 0.5. The structure[20] of the vanadium oxo sulfato complex ion $(VO)_2O(SO_4)_4^{4-}$ is shown in Figure 4. This complex seems to predominate[22, 23] in a very large composition range of all of the binary systems, including the range = 0.20–0.33 used for industrial SO_2 oxidation catalysts.

Heat of mixing in the systems $M_2S_2O_7$-V_2O_5 and $M_2S_2O_7$ -M_2SO_4-V_2O_5 (M = K or Cs) in O_2, SO_2 or Ar

The heat of reactions forming the catalytic active vanadium oxo sulfato complexes and the heat of reactions involved in redox processes and sulfato complex reactions of these species have been measured by calorimetry. Both the indirect and the direct drop method were used to measure the liquid-liquid heat of mixing in the various systems. For the $M_2S_2O_7$-V_2O_5 systems (M = K and Cs) the heat of mixing has been obtained at several temperatures in the range 400–470°C[6, 24] and in the composition region V_2O_5 = 0 - 0.5 in Ar, O_2 or SO_2 atmospheres. The reaction between the two components is very exothermic as illustrated by the measured values of the limiting partial molar enthalpies, i.e. the reaction enthalpies for the formation of the dimeric complex $(VO)_2O(SO_4)_4^{4-}$, as given in Table III. The formulas for the complexes given in Table III are all based on previous electrochemical, spectroscopic and structural

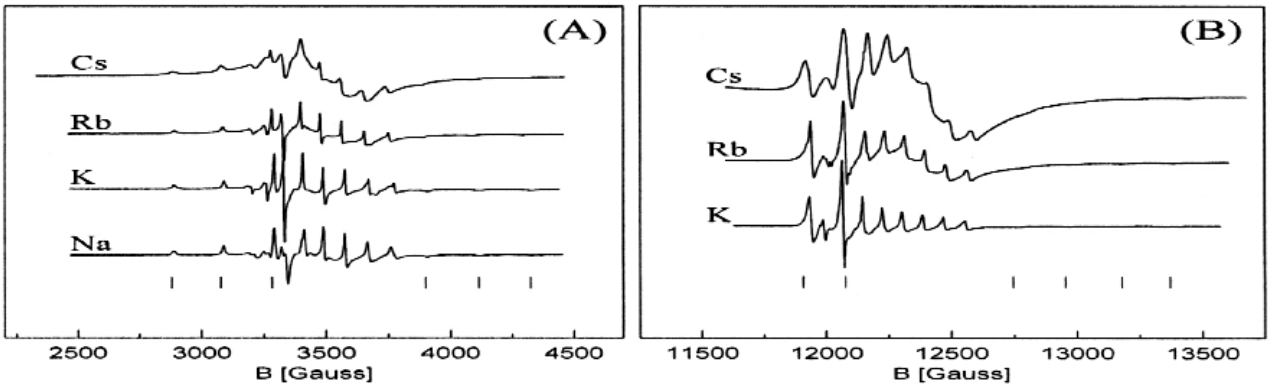

Figure 6. X-band (A) and Q-band (B) EPR spectra of $VO(SO_4)_2^{2-}$ in the $M_2S_2O_7$-V_2O_5/SO_2(g) system with M/V = 160. All spectra are recorded at room temperature. Parallel features are indicated by "|" below the spectra

investigations[3,25,26] and will not be questioned here. From these four obtained reaction enthalpies, the enthalpies of the last four complex reactions can be calculated as indicated in the table. Again, reactions involving reductions by SO_2 are the most exothermic.

EPR spectroscopy characterization of V_2O_5-$M_2S_2O_7$-M_2SO_4/SO_2(g) (M = Na, K, Rb, Cs)

The composition and structure of the V(IV) complexes in pyrosulfate melts were investigated by EPR spectroscopy. Based on the discussion above and an investigation on V(IV) in pyrosulfate[25], the following reactions will be considered for the rest of the discussion:

Dissolution:

$$V_2O_5 + 2S_2O_7^{2-} - (VO)_2O(SO_4)_4^{4-} \qquad [3]$$

Reduction:

$$(VO)_2O(SO_4)_4^{4-} + SO_2 - 2VO(SO_4)_2^{2-} + SO_3 \qquad [4]$$

Furthermore, in the presence of excess sulfate the V(IV) complex will coordinate one additional sulfate:

Complex reaction:

$$VO(SO_4)_2^{2-} + SO_4^{2-} - VO(SO_4)_3^{4-} \qquad [5]$$

At the applied SO_2 pressure the equilibrium Equation 4 is almost completely shifted to the right, i.e. towards V(IV). Figure 5 shows the EPR spectra of samples with M/V = 40, 80 and 160 recorded in the X- and Q-band. All spectra are recorded at room temperature, except for the samples with M/V = 160 which in addition are recorded in the X-band in the molten state at 450–460ºC. The Q-band spectra of the samples with M/V = 160 have been simulated using the Simpow computer program.

The general EPR features of the quenched samples are quite similar with two general trends. The X- and Q-band spectra both show axial symmetry typical for octahedral VO^{2+} complexes with the hyperfine structure (due to coupling to the ^{51}V nucleus, I = 7/2), best resolved in the Q-band spectra. The line width of the spectra increases with increasing vanadium concentration (lower M/V ratio) and with the molar weight of the alkali cation. The samples Rb/V = 40, Rb/V = 80, Cs/V = 40 and Cs/V = 80 could not be recorded with well-resolved hyperfine structure in the X-band and are therefore not shown in Figure 5. The quenched spectra are typical immobilized axial symmetric spectra also known from, e.g. frozen vanadyl containing Schiff bases. Axial symmetric spectra can be well characterized by gtensors and hyperfine coupling constants, i.e. the parameters $g_{\perp\perp}$, $g_{\perp}$, $a_{\perp\perp}$, $a_{\perp}$ and one line width.

The Q-band spectra, stipulated in Figure 5, are computer simulations using these five parameters and assuming Lorentzian line shapes. No differences were found in the parameters dependent on the vanadium concentration (within experimental error), hence the best resolved spectrum for each alkali metal was used for the accurate calculation of the EPR parameters, regardless of the concentration. The quenched samples are identical within the experimental error of ±0.005 and ±10 for g and a respectively, i.e. $g_{\perp\perp}$ = 1.930, $g_{\perp}$ = 1.980, $a_{\perp\perp}$ = 200 Gauss, $a_{\perp}$ = 70 Gauss. Only the parameters of the parallel feature for the Cs-based samples deviate slightly.

It should be stressed, that observable in-plane anisotropy rarely occurs in EPR spectra, even though some rhombicity is present. However, the line width changes significantly by increasing size of the cation. The high temperature X-band EPR spectra (Figure 5) of the molten samples with M/V = 160 exhibit eight isotropic lines of varying intensity as always found for monomeric vanadyl complexes in solution. The different alkali pyrosulfate solvents seem not to affect the first coordination sphere of the complex.

Thus no variation in the isotropic g value or the isotropic hyperfine structure constant is observed as with respect to the type of the alkali cation. In some of the spectra, a skew baseline can be seen, probably due to part formation of dimeric or polymeric V(IV) species where coupling along the chains may smear out the hyperfine structure. The measured isotropic parameters fit well with the calculated isotropic values from the quenched samples considering the large temperature difference, indicating that we are dealing with the same complex in both phases.

The X- and Q-band EPR spectra of the vanadyl complexes without sulfate saturation are shown in Figure 6. The spectra represent axial symmetric complexes as in the sulfate saturated system, but the line width is much smaller, 6-15 G versus 20-50 G for samples with sulfate saturation. This indicates that there is less distortion of the VO^{2+} unit for $VO(SO_4)_2^{2-}$ compared to $VO(SO_4)_3^{4-}$ complexes present in the sulfate saturated system. Furthermore, the EPR parameters of the parallel features are—not surprisingly—changed. The value of $g_{\perp\perp}$ is calculated to be typically

about 0.007 smaller in the case of $VO(SO_4)_2^{2-}$ compared to $VO(SO_4)_3^{4-}$. The perpendicular components are less affected. This shows that the character of the V=O bond is important for the relaxation path of the unpaired electron. This system seems to show the same trend on line width versus alkali metal as the sulfate saturated system, and even more pronounced, again indicating that the vanadyl unit $VO(SO_4)_2^{2-}$ complex is much less distorted than $VO(SO_4)_3^{4-}$.

Relation to catalysis and vanadium containing boiler deposits

During the catalytic oxidation of SO_2 to SO_3 the sulfate activity in the catalyst melt is of course lowered due to the reaction $SO_3 + SO_4^{2-} - S_2O_7^{2-}$ being shifted to the right. At last bed conditions in sulfuric acid production the temperature is in the range 420–450ºC which further stabilizes the $S_2O_7^{2-}$ ion. Therefore, the $M_2S_2O_7$-V_2O_5 system and the redox reaction

$$(VO)_2O(SO_4)_4^{4-} + SO_2 - 2VO(SO_4)_2^{2-} + SO_3 \qquad [6]$$

where SO_3 probably is solvated by $S_2O_7^{2-}$ forming $S_3O_{10}^{2-}$, seem particularly important. This reaction (Equation 6) has been studied spectroscopically for the K-system[27] in the temperature range 435–480ºC and a reaction enthalpy of–107 ± 4kJ/mol was obtained in good agreement with the calorimetric value of -91 ± 20 kJ/mol found here.

However, in the recently published reaction mechanism for SO_2 oxidation by alkali promoted vanadium based catalysts[3] it is proposed that the reaction (Equation 6) is responsible for the deactivation of the catalyst while the catalytic cycle leading to the product probably only involves highly reactive V(V) complexes in rather low concentrations. Therefore, heat of reactions involving those individual V(V) complexes in the cycle cannot easily be obtained. The overall heat of reaction going through the catalytic cycle is of course not different from the heat of the oxidation $SO_2 + {}^1/_2\ O_2 - SO_3$, i.e. $\Delta H^o = -98$ kJ/mol.

The mechanism suggested in reference 3 has to be extended, thus a branch with the formation of the V(V) complex $VO(SO_4)_2^-$ at high SO_3 partial pressures should be included based on previous isolation of this compound from the $K_2S_2O_7$ - V_2O_5-SO_3 system[28, 29]. This step may explain the inhibiting effect of SO_3 on the reaction rate observed experimentally as a negative kinetic reaction order for SO_3[30].

Calorimetric measurements of the heat of reactions in the $M_2S_2O_7$-V_2O_5 system in SO_3 atmosphere are planned as future work. In addition to catalysis, the present work also relates to the chemistry of fireside deposits of boilers fired with vanadium containing fuels like heavy fuel oil and Orimulsion[31]. This paper reviews especially previous thermal and ESR-spectroscopic work[32,33]

Conclusion

Thermal and EPR-spectroscopic measurements have been performed on the molten salts or binary molten salt systems $MHSO_4$, $M_2S_2O_7$, $MHSO_4$-$M_2S_2O_7$ in addition to the SO_2-oxidation catalyst model systems $M_2S_2O_7$-V_2O_5 and $M_2S_2O_7$-M_2SO_4-V_2O_5 in O_2-, SO_2- or Ar-gas atmospheres (M=alkali metal) at temperatures up to 470ºC. Fundamental physico-chemical properties of these molten salt systems have been considered of importance for process design using these media e.g. catalysis and metallurgical processing. Also the transition metal complex formation has been exemplified by vanadium where oxo sulfato V(V) and V(IV) complexes have been identified and redox equilibria involving these complexes have been formulated. The possible role of these complexes for the reaction mechanism of catalytic SO_2 oxidation and the chemistry of deposits in power plant boilers has also been discussed.

Acknowledgement

This work has been partly supported by NATO (SFP 971984) and the Danish Technical Research Council.

References

1. BOGHOSIAN, S., FEHRMANN, R., BJERRUM N.J. and PAPATHEODOROU, G.N. *J. Catal*. vol. 119, 1989 p. 121.
2. ERIKSEN, K.M., KARYDIS, D.A., BOGHOSIAN, S. and FEHRMANN, R. *J. Catal* vol. 155, 1995 p. 32.
3. LAPINA, O.B., BAL'ZHINIMAEV, B.S., BOGHOSIAN, S., ERIKSEN, K.M. and FEHRMANN, R., *Catal. Today* vol. 51, 1999 p. 469.
4. FOLKMANN, G.E., HATEM, G., FEHRMANN, R., GAUNE-ESCARD, M. and BJERRUM, N.J. *Inorg. Chem*. vol. 30, 1991 p. 4057.
5. FEHRMANN, R., HANSEN, N.H. and BJERRUM, N.J. *Inorg. Chem*. vol. 22, 1983 p. 4009.
6. FOLKMANN, G.E., HATEM, G., FEHRMANN, R., GAUNE-ESCARD, M. and BJERRUM, N.J. *Inorg. Chem*. vol. 32, 1993. p. 1559.
7. GAUNE-ESCARD, M. in: R. Gale, D.G. Lovering (eds), *Molten Salt Techniques*, Plenum Press, New York 1991.
8. KUBASCHEWSKI, O. and EVANS, E.L. Metallurgical Thermochemistry, 3rd edn., Pergamon Press, London 1958.
9. National Bureau of Standards, JANAF Thermochemical Tables, 2nd edn., Washington D.C. 1971 suppl. 1974.
10. GAUNE-ESCARD, M., BOGACZ, A., Rycerz L. and SZCZEPANIAK, W. J. *Alloys Comp*. vol. 235, 1996. p. 176.
11. SETARAM DSC 121 - Experimentations, B/03NEDSCF.
12. HATEM, G., ABDOUN, F., GAUNE-ESCARD, M., ERIKSEN K.M. and FEHRMANN, R. *Thermochimica Acta* vol. 319, 1998. p. 33.
13. ERIKSEN, K.M., FEHRMANN, R., HATEM, G., GAUNE-ESCARD, M., LAPINA O.B. and MASTIKHIN, V.M. *J. Phys. Chem*. vol. 100, 1996. p. 10771.
14. SPITSYN, V.I. and MEEROV, M.A. *J. Gen. Chem*. (Engl. Transl.) vol. 22, 1952 p. 963.
15. RASMUSSEN, S.B., ERIKSEN, K.M., HATEM, G., DA SILVA, F. STÅHL, K. and FEHRMANN, R. *J. Phys. Chem*. vol. 105, 2001. p. 2747.
16. HAGISAWA, T. and TAKAI, T. *Sci. Papers Inst. Phys. Chem. Soc*. vol. 31, 1937. p. 677.
17. CAMBI, L. and BOZZA, G. *Ann. Chim. Appl*. vol. 13, 1923. p. 221.

18. FOLKMANN, G.E., ERIKSEN, K.M., FEHRMANN, R., GAUNE-ESCARD, M., HATEM, G., LAPINA, O.B. and TERSKIKH, V. *J. Phys. Chem*. vol. 102, 1998. p. 24.
19. ABDOUN, F., HATEM, G., GAUNE-ESCARD, M., ERIKSEN K.M. and FEHRMANN, R. *J. Phys. Chem*. vol. 18, 1999. p. 3559.
20. NIELSEN, K., FEHRMANN, R. and ERIKSEN, K.M. *Inorg. Chem*. vol. 32, 1993. p. 4825.
21. NIELSEN, K., ERIKSEN, K.M. and FEHRMANN, R. in prep.
22. BOGHOSIAN, S., BORUP F. and CHRISSANTHOPOULOS, A. *Catal. Lett*. vol. 48, 1997. p. 145.
23. BOGHOSIAN, S., CHRISSANTHOPOULOS, A. and FEHRMANN, R. *J. Phys. Chem*., vol. 106, 2002. p. 49.
24. FEHRMANN, R., GAUNE-ESCARD, M. and BJERRUM, N.J. *Inorg. Chem*. vol. 25, 1986. p. 1132.
25. RASMUSSEN, S.B., ERIKSEN, K.M. and FEHRMANN, R. *J. Phys. Chem*. vol. 103, 1999. p. 11282.
26. HATEM, G., ERIKSEN, K.M. and FEHRMANN, R. *Thermochimica Acta*, vol. 379, 2001. p. 187.
27. KARYDIS, D.A., ERIKSEN, K.M., FEHRMANN, R. and BOGHOSIAN, S. *J. Chem. Soc*. Dalton Trans. 1994. p. 2151.
28. RICHTER, K.-L. and MATTES, R. Z. *Anorg. Allg*. Chem. vol. 611, 1992. p. 158.
29. POULSEN, A. and NIELSEN, K. unpublished results.
30. URBANK, A. and TRELA, M. *Catal. Rev. - Sci. Eng*. vol. 21, 1980. p. 73.
31. RASMUSSEN, S.B., HAGEN, S.U., MASTERS, S. G., HAGEN, A., STAHL, K., ERIKSEN, K.M., SIMONSEN, P., JENSEN, J.N., BERG, M., FEHRMANN, R. and CHORKENDORFF, I. *Power Plant Chem*., 5 (2003) 360.
32. HATEM, G., ERIKSEN, K.M., GAUNE-ESCARD, M. and FEHRMANN, R. Topics in Catal., vol. 19, 2002. p. 325.
33. RASMUSSEN, S.B., ERIKSEN, K.M. and FEHRMANN, R. *J. Chem. Soc*. Dalton Trans., 2002, p. 87.